J Electroceram (2010) 24:200–204
DOI 10.1007/s10832-008-9555-6

Size-dependent photovoltaic property in hollow hemisphere array based dye-sensitized solar cells

Dae-Jin Yang · Su-Chul Yang · Jae-Min Hong · Hyunjung Lee · Il-Doo Kim

Received: 9 May 2008 / Accepted: 25 September 2008 / Published online: 16 October 2008

Abstract For a working electrode in dye-sensitized solar cells (DSSCs), an anatase TiO_2 electrode with a hollow hemisphere structure (with diameters of 0.4, 1.5, and 5.0 μm) was fabricated using colloidal templating and RF-sputtering techniques. The experimental results of a short-circuit current density of 1.96 mA/cm^2, an open-circuit voltage of 0.73 V, and a power conversion efficiency (AM 1.5) of 0.67% were obtained with a shell thickness of 300 nm, a hemisphere diameter of 0.4 μm, and a 100 nm thick blocking layer. The microstructural features, i.e. hemisphere diameter and shell thickness, played an important role in promoting the charge-collection ability.

Keywords Photovoltaic · Hollow hemisphere · TiO_2

Dye-sensitized solar cells (DSSCs) based on a dye coupled TiO_2 offer unique opportunities as renewable energy sources due to their potential to replace Si-based solar cells. In particular, DSSCs can provide several attractive features including a low cost, environmental friendliness, and large scale production [1, 2]. Thus far, DSSCs with a power conversion efficiency (AM1.5) of ~11% have been demonstrated using nanocrystalline TiO_2 powders followed by a $TiCl_4$ treatment, anti-reflecting coating, or inserted scattering-layer [3–5]. Although encouraging progress has been made, the current achieved power conversion efficiency is still below the theoretical value [6]. In randomly packed TiO_2 nanocrystalline films, it is expected that electron transport is limited largely by the residence time of electrons in traps and by structural disorder at the contact between two nanoparticles [7–10]. However, a strongly interconnected architecture offers significantly superior electron transportability [11–13]. It is important to note that the electron diffusion coefficient for a dense TiO_2 thin film is much higher than that of nanocrystalline TiO_2 [14]. However, the small surface-to-volume ratio of dense TiO_2 thin film often limits the amount of adsorbed dye molecules. Therefore, a strongly interconnected morphology with a sufficient surface area is highly desirable for the working electrode in DSSCs [11–13, 15–17]. To satisfy these criteria, a new type of hollow TiO_2 hemisphere structure that effectively absorbs the dye molecule and achieves a high photocurrent has been reported recently [18]. The present work targets a further elucidation of the influence of dimensional factors, i.e. the hemisphere diameter, shell thickness, and blocking layer on photovoltaic properties.

For the blocking layer (BL), 100 nm thick TiO_2 thin film was deposited on SnO_2:F (FTO) coated glass substrates. An aqueous colloidal solution of poly(methyl methacrylate) (PMMA) microspheres with diameters of 0.4, 1.5, and 5.0 μm (Soken Chemical & Engineering Co., Ltd.), ultrasonically dispersed in deionized water and ethanol, was spin coated at spin speeds of 600 to 1,000 rpm onto BL/FTO/glass substrates and dried overnight in a desiccator at room temperature. After that, a quasi-ordered colloidal array was formed. Subsequently, 100 and 300 nm thick TiO_2 films were deposited over the single layered PMMA microsphere templates. The TiO_2 deposition was performed

D.-J. Yang · J.-M. Hong · I.-D. Kim (✉)
Center for Energy Materials Research,
Korea Institute of Science and Technology,
P.O. Box 131, Cheongryang, Seoul 130-650, Republic of Korea
e-mail: idkim@kist.re.kr

S.-C. Yang · H. Lee
Hybrid Materials Research Center,
Korea Institute of Science and Technology,
P.O. Box 131, Cheongryang, Seoul 130-650, Republic of Korea

H. Lee
e-mail: lhj0630@kist.re.kr

via RF-sputtering under the following conditions: a power of 85 W, a working pressure of 10 mTorr, and an Ar flow of 10 sccm. No heating was applied to the substrates during the film deposition to prevent the decomposition of PMMA in the sputtering chamber. Following the TiO_2 film sputter deposition, the samples were calcined in air at 450 °C for 30 min to induce the crystallinity of TiO_2 films, as well as to decompose the PMMA templates. The PMMA template decomposed during calcination [18]. X-ray diffraction (XRD, D/MAX-2500, Rigaku), scanning electron microscopy (SEM, JSM-6330F, JEOL), and high resolution transmittance electron microscopy (HR-TEM, Tecnai G2, FEI Hong Kong Co. Ltd.) were used to examine the phase composition and microstructure of the films. The TiO_2 hollow hemisphere electrode was immersed overnight in an ethanolic solution containing 3×10^{-4} M of N3 ruthenium dye (Solaronix). The electrode was rinsed with ethanol and dried at room temperature. The liquid electrolyte consisted of 0.6 M 1-hexyl-2,3-dimethyl-imidazolium iodide (C6DMIm), 0.05 M iodine (I_2), 0.1 M lithium iodide (LiI), and 0.5 M 4-tertbutylpyridine dissolved in 3-methoxyacetonitrile. The Pt counter electrode was prepared by spin-coating a H_2PtCl_6 solution (7 mM in isopropyl alcohol) on the FTO glass and sintered at 450 °C for 30 min. The typical active area of the DSSC was 0.16 cm^2. The photocurrent–voltage characteristics were measured with a Keithley 2400 SMU under a global AM1.5, 100 mW/cm^2 irradiation.

Figure 1(a) shows a SEM micrograph of a single layered PMMA colloidal array on the FTO/glass substrate prepared using microspheres with a diameter of 1.5 μm. This quasi-ordered array was hexagonally close-packed. Figures 1(b) and (c) are the SEM images of the top view and cross-sectional view of the TiO_2 hollow hemispheres after 100 nm thick TiO_2 sputtering onto a PMMA colloidal array at room temperature and calcination at 450 °C, respectively. The diameter of the individual hemisphere was commensurate with that of the original PMMA microspheres. The hemisphere height was approximately 1 μm as shown in Fig. 1(c). Figure 1(d) emphasizes the hollow shape of the TiO_2 hemisphere. This SEM image was taken from a mechanically scraped sample. The shell thickness was approximately 100 nm. One can see "burst holes" positioned at the bottom of hemispheres, that were produced as a result of PMMA decomposition during calcinations. These open holes enable easy penetration of N3 dyes and electrolytes into the inner space of hollow structures [18]. This unique morphology is expected to

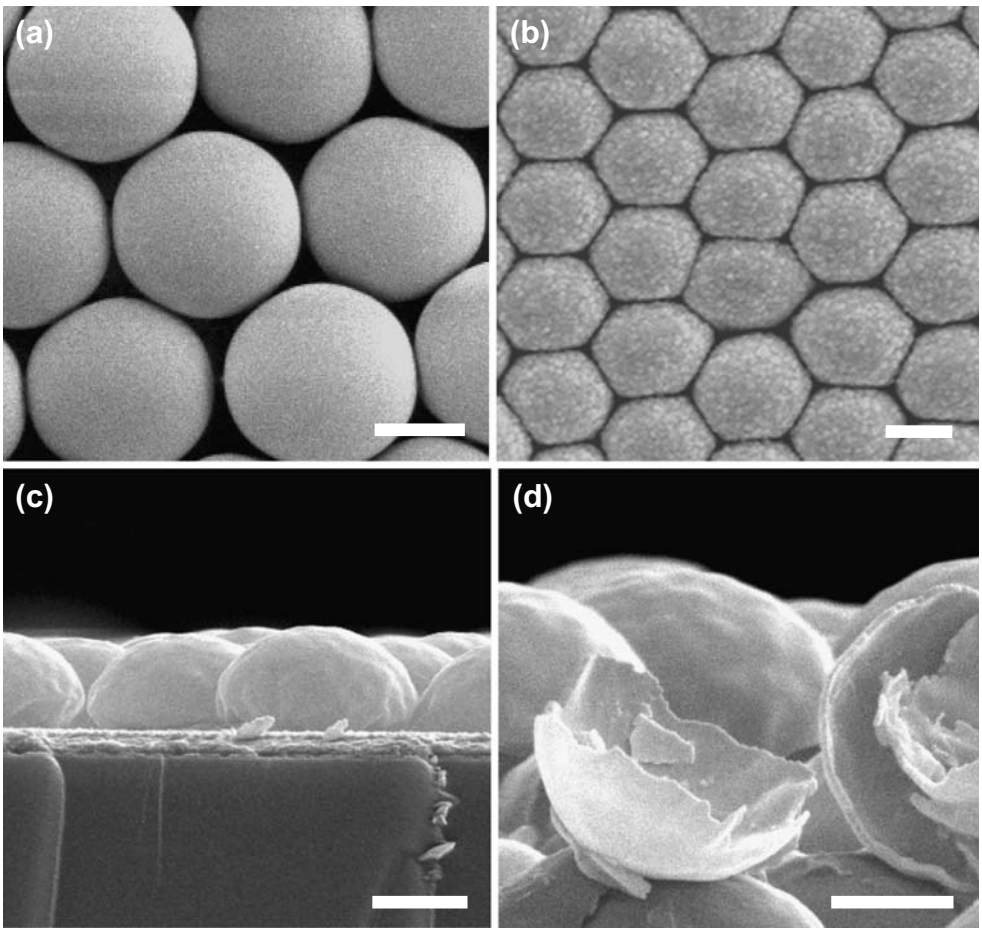

Fig. 1 SEM images of the as-prepared electrode; (**a**) a single layered PMMA colloidal array template, (**b**) top and (**c**) side views of the TiO_2 hollow hemisphere array electrode, (**d**) tilted view of mechanically scraped sample. All scale bars represent 1 μm

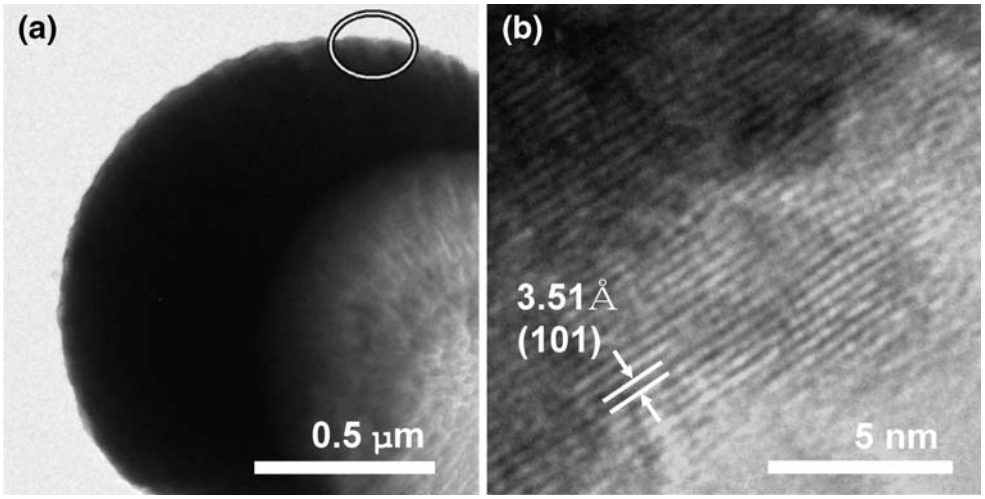

Fig. 2 Microstructure of sample obtained after calcination of TiO_2 hollow hemisphere; (**a**) bright-field TEM image of the individual hemisphere (**b**) HR-TEM image of the marked region in (**a**)

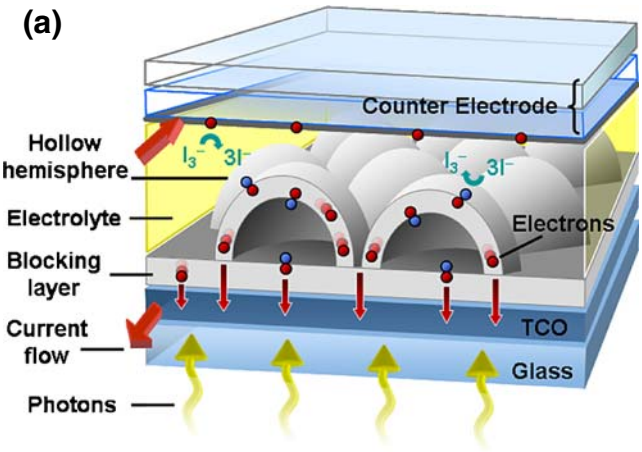

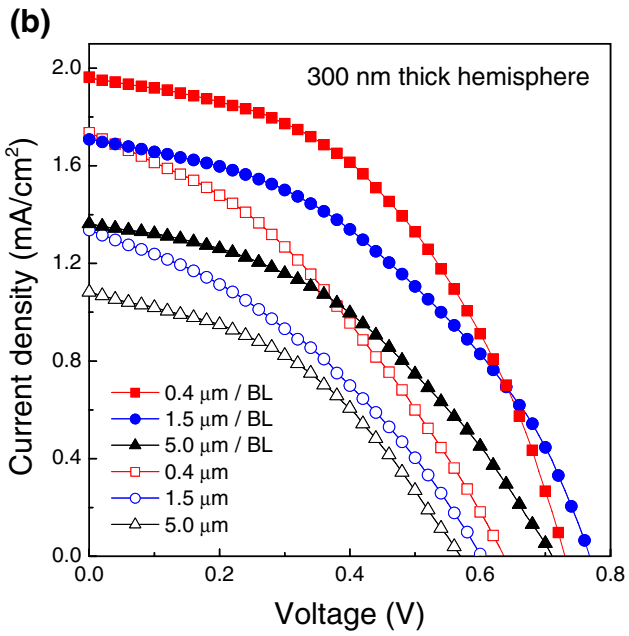

Fig. 3 (**a**) Illustration of the device configuration, current flow, and the direction of illumination. (**b**) Current–voltage characteristics of a DSSC using TiO_2 hollow hemisphere with and without blocking layers

increase the amount of adsorbed N3 dye due to the enhanced surface area (outer and inner surfaces, plus the geometric effect of the hemisphere). At the same time, the strongly interconnected photoanode architecture offers potential to improve electron transport. Both effects have a significant influence on the overall efficiency of DSSCs.

In order to investigate the microstructure and composition of the hollow hemispheres, a HR-TEM analysis and XRD measurement were performed. Figure 2(a) shows the TEM micrographs of a single TiO_2 hemisphere. As shown in Fig. 2(b), the HR-TEM image showed that the individual TiO_2 hemispheres had a lattice spacing of 3.51 Å consistent with the [101] direction in anatase TiO_2. The XRD analysis confirmed that the TiO_2 films had a single-phase polycrystalline anatase structure with the preferred (101) direction and evidence of (200) orientation (not shown here) [18].

Figure 3(a) illustrates the cross-sectional geometry of a hollow hemisphere DSSC. In the liquid-type DSSC, the photo-injected electrons from dye molecules can react with the I_3^-/I^- in the electrolyte [19]. Thus, the use of an additional blocking TiO_2 layer is essential to minimize

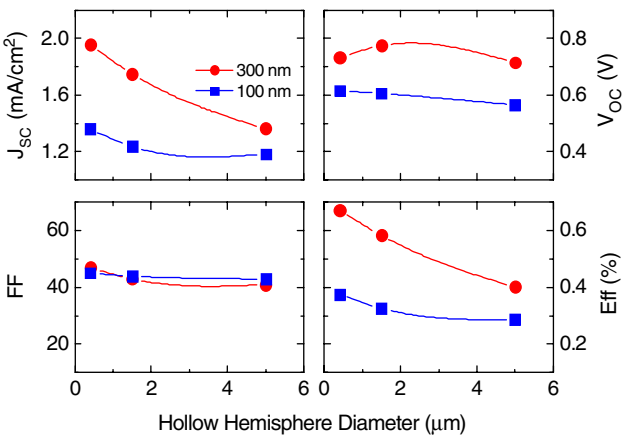

Fig. 4 Current–voltage characteristics for different shell thicknesses (100, 300 nm) and hemisphere diameters (0.4, 1.5, and 5.0 μm)

current loss through recombination at the FTO/electrolyte interface. The introduction of such a dense TiO_2 blocking layer between the hollow hemisphere TiO_2 layer and FTO electrode clearly enhanced the photocurrent and photovoltage output, as shown in Fig. 3(b). At 100% sun, the TiO_2 electrode with a shell thickness of 300 nm, a hemisphere diameter of 0.4 μm, and a 100 nm thick blocking layer, exhibited a short circuit current density (J_{sc}) of 1.96 mA/cm^2, an open circuit voltage (V_{oc}) of 0.73 V, and a fill factor (FF) of 0.47, with an overall conversion efficiency (Eff) of 0.67%. However, the sample without the blocking layer exhibited a lower J_{sc} of 1.73 mA/cm^2, V_{oc} of 0.64 V, FF of 0.36, and Eff of 0.39%. All DSSCs fabricated on the blocking layer exhibited a greatly enhanced performance compared with the cells without blocking layers. It is apparent that the blocking layer deposited via the sputtering method effectively blocked the backward flow of electrons from the FTO to the electrolyte.

Figure 4 represents the structural dependence of the cell performance as a function of shell thickness and hemisphere diameter. (All samples in Fig. 4 have blocking layers.) The DSSCs with 300 nm thick TiO_2 hollow electrodes regardless of hemisphere sizes exhibited a higher J_{sc}, V_{oc}, and Eff compared with the DSSCs using 100 nm thick TiO_2 hemisphere electrodes. In general, during the sputtering deposition, the surface morphology became rougher as the thickness of the thin film increased [20]. The rougher surface morphology could induce a higher adsorption of the N3 dye, thus leading to an improved photon absorption and carrier generation. Furthermore, the J_{sc} value of the DSSCs increased as the hemisphere diameter decreased, leading to an enhanced Eff up to 0.67%. This behavior is very interesting compared with that of conventional TiO_2 nanocrystalline films. In the nanocrystalline structure, a larger quantity of dye can be adsorbed in thicker films due to the larger surface area, leading to an improved photocurrent with an increased film thickness (up to ~10 μm) [4]. However, for the hollow hemisphere structure, the calculated surface area in the unit area is almost constant, regardless of the hemispherical diameter. To calculate the surface/contact area simply, it was assumed that all hollow hemispheres were hexagonally packed and no diameter shrinkage occurred after the heat treatment. On the other hand, the distance from hemisphere bottom to apex became shorter as the hemisphere diameter decreased. A shorter average electron-travelling distance in hemispheres with smaller diameter could reduce the current loss by minimizing the recombination probability while the injected electrons traverse along the TiO_2 electrode. As a result, a higher charge collection ability can be achieved by decreasing the hollow hemisphere size although surface area remains constant.

In summary, DSSC working electrodes based on TiO_2 hollow hemisphere arrays were fabricated by combining the chemical and physical synthesis routes, i.e. using the colloidal templating technique. The resultant TiO_2 hemisphere films had a unique morphology that was simultaneously strongly interconnected and had a high surface area. Inserting a compact TiO_2 blocking layer effectively blocked the backward flow of electrons from the FTO to the electrolyte, resulting in improved cell performance. The experiments verified that the dimension of the hollow hemisphere, i.e. shell thickness and hemisphere diameter, were important parameters in DSSC performance. As the shell thickness increased, the overall conversion efficiency improved. In particular, compared with conventional TiO_2 nanocrystalline films, most cell performances increased as the hollow hemisphere size decreased. Although the overall conversion efficiency was lower compared with the conventional nanoparticle based DSSCs, it is expected that the hollow hemisphere structure is a good model for further systematic understanding of the structure correlations in the DSSC properties for the fabrication of working electrodes.

Acknowledgement This work was supported by KIST Independent Project of one of the authors (I.-D. K).

References

1. B. O'Regan, M. Grätzel, Nature **353**, 737 (1991) doi:10.1038/353737a0
2. P. Wang, S.M. Zakeeruddin, J.E. Moser, M.K. Nazeeruddin, T. Sekiguchi, M. Grätzel, Nat. Mater. **2**, 498 (2003)
3. Y. Chiba, A. Islam, R. Komiya, N. Koide, L. Han, Appl. Phys. Lett. **88**, 223505 (2006) doi:10.1063/1.2208920
4. M.K. Nazeeruddin, P. Pechy, T. Renouard, S.M. Zakeeruddin, R. Humphry-Baker, P. Comte, P. Liska, L. Cevey, E. Costa, V. Shklover, L. Spiccia, G.B. Deacon, C.A. Bignozzi, M. Grätzel, J. Am. Chem. Soc. **123**, 1613 (2001) doi:10.1021/ja003299u
5. S. Ito, S.M. Zakeeruddin, R. Humphry-Baker, P. Liska, R. Charvet, P. Comte, M.K. Nazeeruddin, P. Péchy, M. Takata, H. Miura, S. Uchida, M. Grätzel, Adv. Mater. **18**, 1202 (2006) doi:10.1002/adma.200502540
6. A.J. Frank, N. Kopidakis, J. van de Lagemaat, Coord. Chem. Rev. **248**, 1165 (2004) doi:10.1016/j.ccr.2004.03.015
7. K. Zhu, N.R. Neale, A. Miedaner, A.J. Frank, Nano Lett. **7**, 69 (2007) doi:10.1021/nl062000o
8. Q. Wang, J.E. Moser, M. Grätzel. J. Phys. Chem. B **109**, 14945 (2005) doi:10.1021/jp052768h
9. P.E. deJongh, D. Vanmaekelbergh, Phys. Rev. Lett. **77**, 3427 (1996) doi:10.1103/PhysRevLett.77.3427
10. N. Kopidakis, K.D. Benkstein, J. van de Lagemaat, A.J. Frank, Phys. Rev. B **73**, 045326 (2006) doi:10.1103/PhysRevB.73.045326
11. M. Law, L.E. Greene, J.C. Johnson, R. Saykally, P.D. Yang, Nat. Mater. **4**, 455 (2005) doi:10.1038/nmat1387
12. G.K. Mor, K. Shankar, M. Paulose et al., Nano Lett. **6**, 215 (2006) doi:10.1021/nl052099j
13. A.B.F. Martinson, J.W. Elam, J.T. Hupp et al., Nano Lett. **7**, 2183 (2007) doi:10.1021/nl070160+
14. Q. Wang, S. Ito, M. Grätzel, F. Fabregat-Santiago, J. Ivan Mora-Sero, Bisquert, T. Bessho, H. Imai, J. Phys. Chem. B **110**, 25210 (2006) doi:10.1021/jp064256o

15. H. Wang, C.T. Yip, K.Y. Cheung, A.B. Djurišić, M.H. Xie, Y.H. Leung, W.K. Chan, Appl. Phys. Lett. **89**, 023508 (2006) doi:10.1063/1.2221502
16. M.Y. Song, Y.R. Ahn, S.M. Jo, D.Y. Kim, J.P. Ahn, Appl. Phys. Lett. **87**, 113113 (2005) doi:10.1063/1.2048816
17. M. Gomez, J. Rodriguez, S.E. Lindquist, C.G. Granqvist, Thin Solid Films **342**, 148 (1999) doi:10.1016/S0040-6090(98)01482-5
18. S.C. Yang, D.J. Yang, J.K. Kim, J.M. Hong, H.G. Kim, I.D. Kim, H.J. Lee, Adv. Mater. **20**, 1059 (2008) doi:10.1002/adma.200701808
19. P.J. Cameron, L.M. Peter, J. Phys. Chem. B **107**, 14394 (2003) doi:10.1021/jp030790+
20. S. Ito, P. Liska, P. Comte, R. Charvet, P. Pechy, U. Bach, L. Schmidt-Mende, S.M. Zakeeruddin, A. Kay, M.K. Nazeeruddin, M. Grätzel, Chem. Commun. (Camb.) **34**, 4351 (2005) doi:10.1039/b505718c